SENSORS & TRANSDUCERS

ISSN 1726-5479

vol. 149

2/13

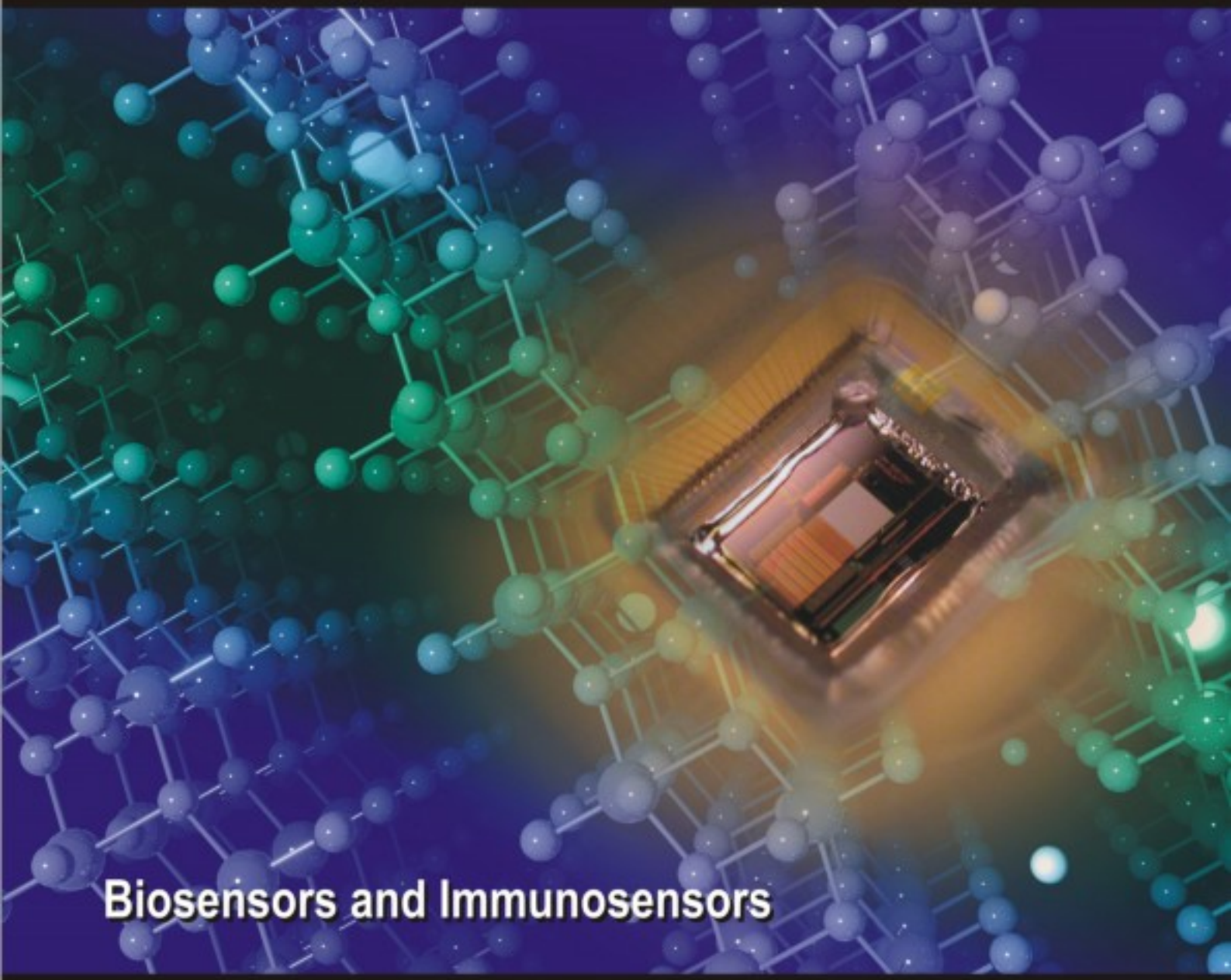

Biosensors and Immunosensors

International Frequency Sensor Association Publishing

IFSA

Printed in the USA.

Sensors & Transducers

Volume 149, Issue 2, February 2013 | **www.sensorsportal.com** | **ISSN 1726-5479**

Sensors & Transducers Journal

Contents

Volume 149
Issue 2
February 2013

www.sensorsportal.com

ISSN 2306-8515
e-ISSN 1726-5479

Research Articles

Authors are encouraged to submit article in MS Word (doc) and Acrobat (pdf) formats by e-mail: editor@sensorsportal.com. Please visit journal's webpage with preparation instructions: http://www.sensorsportal.com/HTML/DIGEST/Submition.htm

International Frequency Sensor Association (IFSA).

Sensors & Transducers, Vol. 149, Issue 2, February 2013, pp. 60-68

Sensors & Transducers

http://www.sensorsportal.com

Surface Plasmon Resonance Biosensor

[1] Nina GRIDINA, [2] Gleb DOROZINSKY, [2] Roman KHRISTOSENKO, [2] Vladimir MASLOV, [2] Anton SAMOYLOV, [2] Yury USHENIN, [2] Yury SHIRSHOV

[1] Institute of neurosurgery n. acad. A. Romodanov AMS of Ukraine,
32, Platona Mayborody st., 04050, Kiev, Ukraine
[2] V. Ye. Lashkaryov Institute of Semiconductor Physics of NAS of Ukraine,
45, Prospekt Nauki, 03028, Kiev, Ukraine
E-mail: vladmaslov@mail.ru

Received: 15 January 2013 /Accepted: 14 February 2013 /Published: 28 February 2013

Abstract: Performed in this paper is numerical modeling of the angular dependence for light reflectivity $R(F)$ in surface plasmon-polariton resonance (SPR) realized in Kretschmann geometry when studying the interface gold/suspension of spherical particles (cells) in the assumption that the dielectric permittivity of particles suspension ε is described by the theory of effective medium. It has been shown that availability of suspended particles in solution inevitably results in appearance of an intermediate layer with the ε gradient between gold surface and suspension bulk, as a result of which the SPR angle shifts to lower values. Near the critical angle, the first derivative dR/dF demonstrates a clearly pronounced peak, which allows determining the ε value for suspension bulk and the ε gradient in the intermediate layer. Obtained in our experiments were SPR curves for two suspensions of erythrocytes – the dense one (erythrocyte mass after centrifuging) and loose solution (whole blood). In the case of erythrocyte mass, fitting the experimental and calculated curves enabled us to quantitatively determine the bulk ε value for this erythrocyte mass (ε_b=1.96), thickness of the intermediate layer d_m (300…400 nm) and ε gradient in the intermediate layer. On the contrary, the SPR curve for whole blood appeared to be close to that of pure plasma. This fact allows only estimation of the thickness d_m~2000...3000 nm as well as minimum ε value in the intermediate layer, which is close to that of plasma (ε = 1.79). Also, discussed is the mechanism of influence of the cell shape near the gold surface on the SPR effect.

Keywords: Surface plasmon-polariton resonance (SPR), Liquid suspensions, Weighted erythrocytes, Biosensor, Blood sensor.

1. Introduction

Surface plasmon resonance (SPR) is a phenomenon which involves the absorption of a p-polarized light by the surface electrons of a metal film (e.g., silver or gold) under specific resonance conditions determined by the dispersion relations of the surface plasmons [1-3]. This resonance condition is extremely sensitive to the refractive index and thickness of the dielectric medium (the medium can be a liquid, gas, or solid) in contact with the metal surface. In the last 20 years, SPR has been

Article number P_1128

extensively studied and developed into a useful technique to probe refractive index and thickness changes which enabled the construction of optical sensors measuring the concentration of chemicals, humidity, pressure, temperature, and biomolecular interactions [4-9].

SPR can be optically excited if the wave vector k_{inc} of the incident light with angular frequency ω has a surface-parallel component k_x equal to the wave vector of the surface plasmon (SP) waves k_{sp}. However, the SP waves cannot be excited by a light directly incident from air onto the interface because energy and momentum conservation cannot be satisfied simultaneously in the frequency range of their dispersion curves. This problem is solved using a dispersive medium (i.e., prism, gratings, etc.) that can enable $k_{inc} > k_{sp}$. Then $k_x = k_{sp}$ can be satisfied by varying the angle of incidence of the light. The incident angle at which the SPR occurs is always higher than that of the total internal reflection for the prism and the bulk medium that form interfaces with the metal. Two basic configurations that use prisms for photon–SP coupling are the Otto and Kretschmann–Raether (KR) configurations [10], [11]. In the Otto configuration, the sample to be sensed is limited with the air gap between the metal and prism. On the other hand, in the KR configuration, the sensing layer is located between the metal layer and air so that the sample is not limited to a very small volume. Therefore, it is more suitable for sensing applications.

If the condition for the excitation of SP waves

$$Re[k_{sp}] = k_{inc} \cdot n_0 \cdot \sin\theta \qquad (1)$$

where $k_{inc} = 2\pi/\lambda$, and n_0 and θ are the refractive index of the prism and the angle of the incidence, respectively, is analyzed, it can be seen that there are two parameters, namely, θ and λ that can be controlled or modulated to excite SP waves. The excitation of the SPR is understood by observing the reflected light spectrum obtained either by "angular interrogation" or "wavelength interrogation." In the angular interrogation approach λ, of the incident light is kept constant and θ is varied. At a specific θ, the incident light is absorbed due to the SPR excitation, resulting in a sharp dip in the reflected light spectrum. This spectrum is characterized by three parameters: resonance angle θ_{min}, half width at half maximum $\Delta\theta$, and the reflection minimum R_{min} (see Fig. 1). In the wavelength interrogation approach, wavelength λ of the incident light is varied while the incidence angle is kept constant. At $\lambda = \lambda_{min}$, resonance condition is achieved and this is understood with a dip in SPR spectrum. In this approach, parameters which are used to characterize the spectrum are resonance angle λ_{min}, half width $\Delta\lambda$, and reflection minimum R_{min}. SPR sensors generally use the following detection approaches: 1) measurement of resonant angle shift; 2) measurement of resonant wavelength shift; and 3) measurement of change in light intensity.

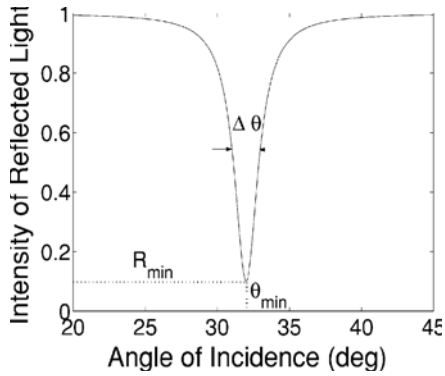

Fig. 1. Illustration of the SPR spectrum with angular interrogation approach. θ_{min} : SP resonance coupling angle. $\Delta\theta$: SP half width. R_{min} : intensity of the reflected light in the resonance condition.

2. Estimation of the Influence of Erythrocyte Volume Fraction on the SPR Effect

The widely used physical model capable to describe the response inherent to dredge of micro- and nano-particles on harmonic electromagnetic excitation is the so-called "approximation of effective medium" by Bruggeman [12-15]. In accord with this approximation, the complex dielectric permittivity ε of a mixture consisting of k components is related with dielectric permittivities of components ε_k and their partial volumes q_k in the following manner:

$$\Sigma q_k(\varepsilon_k-\varepsilon)/(\varepsilon_k+2\varepsilon) = 0;\ \Sigma q_k = 1 \qquad (2)$$

Let us assume that the dielectric permittivity of the studied suspension obeys this rule, and the number of components in this mixture is equal to two: one of the components is transparent liquid (blood plasma) with the dielectric permittivity $\varepsilon_s \sim 1.8$ [16], and the second one – erythrocytes as micro-spheres with the radius R, which are filled with haemoglobin possessing the dielectric permittivity $\varepsilon_e \sim 2.07$ [16, 17]. For definiteness, let us take that micro-spheres are packed on the gold surface in some quadratic manner, as shown in Fig. 2. The micro-spheres touch the gold surface, and space between them is filled with liquid.

To qualitatively describe the SPR effect in this system, let us represent the space above the gold surface as a stack of N thin layers, each of which possesses the thickness δ (Fig.2, middle). It is obvious that the haemoglobin fraction in each layer inside the elementary area $4R^2$ is equal to $\pi\rho^2\delta$, while ρ increases from zero (when $x = 0$) up to R (when $x = R = d_m$).

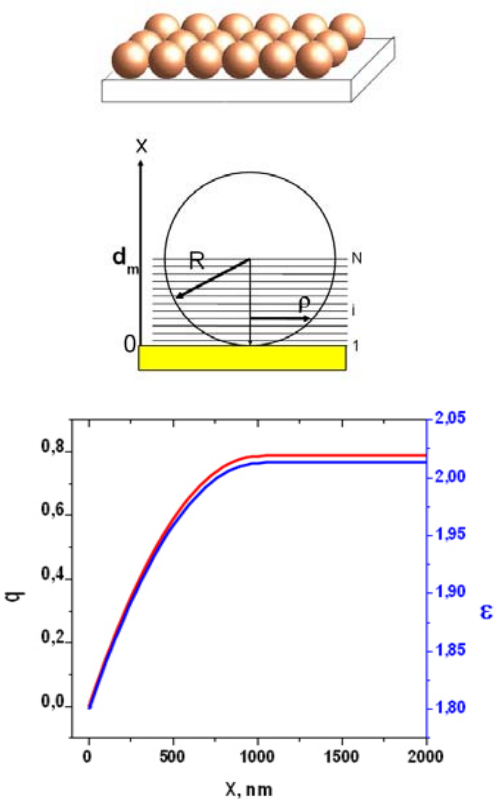

Fig. 2. Microspheres on the gold surface (top) and geometry of model (middle); Bottom: dependences for set of microspheres R=1000 nm filling factor q(x) and dielectrical permittivity ε(x).

Let us consider that for $x > d_m$ the factor of filling q reaches the bulk value $\pi/4 = 0.785$. The calculated dependence $q(x)$ for micro-spheres with the radius $R = 1000$ nm is shown in Fig. 2 (bottom). Shown in the same place is the dependence $\varepsilon(x)$ for mixture, which is calculated using the formula (2). It is seen that in this model the ε value is monotonously increased up to the bulk value 2.01 for 1000 nm and then remains constant. It can be easily predicted that, in the case of non-dense packing or some deformation of spheres near the surface, the boundary values of q and ε in the curves shown in Fig. 2 will be changed but their general look will be the same. To simplify our calculations, we took the law of changing $\varepsilon(x)$ in the following form:

$$\varepsilon(x) = \varepsilon_s + (\varepsilon_b - \varepsilon_s)\, x d_m \quad for\ 0 < x < d_m;$$
$$\varepsilon(x) = \varepsilon_b \quad for\ x > d_m, \tag{3}$$

and analyze the influence of this layer on the SPR curve. Our calculation of the reflected light relative intensity (R) on the angle of incidence (F) was made for the stack of 15 plates with the total thickness d_m from 50 up to 1200 nm (which corresponds to the increasing radius of micro-spheres). Fig. 3 shows the curves $R(F)$ for gradual increase of the parameter d_m within the above range. It is seen that the angular position F_{min} is shifted to the left (curves 1 to 14) with increasing d_m.

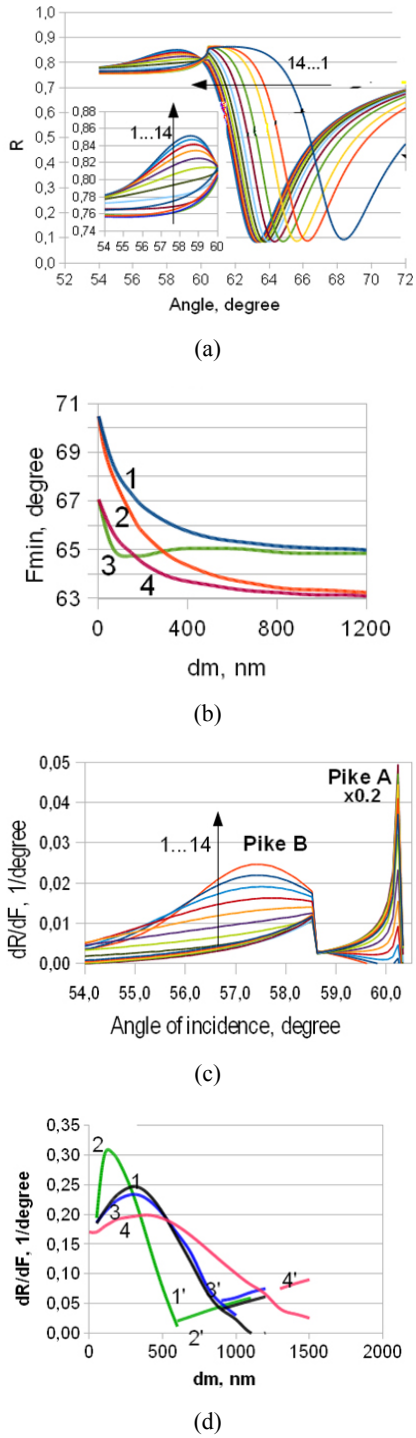

Fig. 3. A) Calculated SPR curves for the stack of 15 plates. Numbers 1...14 correspond such values of d_m : 50, 100, 150, 200, 300, 400, 500, 600, 700, 800, 900, 1000, 1100 и 1200 nm. Shown on the bottom left is part of curve $R(F)$ near the critical angle. B) F_{min} shift against d_m increase at the different values ε_s and ε_b: 1 — ε_s= 1.82, ε_b=1.96; 2 — ε_s=1.77, ε_b=1.96; 3 - ε_s= 1.82, ε_b=1.88; 4 - ε_s=1.77, ε_b=1.88. C) Dependence of derivative dR/dF against incidence angle in the critical angle region. D) A and B peaks amplitudes versus d_m (the scales of curves 1' – 4' are three times multiplied).

The dependence of F_{min} on d_m (that is usually measured in these experiments) is depicted in Fig. 3b for four cases when suspension is a mixture of micro-spheres in various concentrations with two liquids: ε_s = 1.82 (corresponds to blood plasma) and ε_s = 1.77 (corresponds to buffer solution). The curves 1 and 2 are related to the case of dense suspension (q = 0.85), while the curves 3 and 4 – to the case of the loose one (q = 0.45). It is seen that for d_m = 0 the position of F_{min} depends only on q, but not on the liquid phase type.

On the other hand, when the thickness d_m is sufficiently high (800...1200 nm) the value F_{min} is determined only by the liquid type; the transition from initial to final values of F_{min} happens gradually; in the case of the curves 1, 2 and 4 it is monotonous, but in the case of the curve 3 within the range of thicknesses 200 to 400 nm there appears non-monotone. In all the cases, the position of F_{min} looses its sensitivity to the intermediate layer for d_m > 600 nm.

By contrast, the part of the *R(F)* curve near the critical angle demonstrates the most pronounced change for d_m > 600 nm (it corresponds to large sizes of micro-particles) as it is seen in Fig. 3a, the insert on the left. The step in the *R(F)* curve corresponding to the critical angle (60.3 degree for ε_b = 1.96) disappears and arises again (for d_m > 800 nm) in the vicinity of 56 degree. For a more detailed analysis of the *R(F)* curve, let us consider its first derivative *dR/dF* that is shown in Fig. 3c. Within the range 50 < d_m < 600 nm (curves 1 to 7), one can observe one narrow (fractions of degree) peak (peak A) corresponding to the critical angle inherent to the interface glass/suspension (60.33 degree for ε_b = 1.96). Its height changes non-monotonously with growing d_m. Within the range 600 < d_m < 1000 nm (curves 8 to 14), the peak A disappears, however there arises a new wide maximum near 57.3 degree (peak B) (curves 12 to 14). Its height increases for d_m > 1000 nm.

Shown in Fig. 3d is behavior of the amplitude of A and B peaks with increasing the thickness of the intermediate layer d_m for various ε_s and ε_b values. The amplitude of the peak A depends on d_m in non-monotonous manner and possesses the maximum at 0.2…0.3 reciprocal degrees for d_m = 200...300 nm (curves 1 to 4). At the same time, the amplitude of the peak B (curves 1' to 4') increases with growing d_m practically in a linear manner. It is also seen that the peak B arises only for large thicknesses d_m (800 to 1000 nm), and the more is the difference ε_s - ε_b, the lower values of d_m are necessary to register the peak B. Adduced in Table 1 is the angular positions of A and B peaks inherent to suspensions of micro-spheres for above two concentrations in two different liquids. The peak A angle exactly corresponds to the critical angle of the system glass/suspension bulk. Thereof, one can easily calculate the ε_b value. The angular position of B peak is also close to the critical angle of the boundary glass substrate/liquid phase, but exceeds it a little.

Table 1. Angle position of peaks A and B for rations of ε_s, ε_b.

	ε_b=1.96		ε_b=1.88	
	Peak A	Peak B	Peak A	Peak B
ε_s=1.77	60.33	56.61	58.32	56.31
ε_s=1.82	60.33	57.41	58.32	57.01

Two conclusions follow from the said above, namely: 1) availability of A peak in the curve *dR*/*dF* allows determining the value of dielectric permittivity inherent to suspension bulk ε_b, that is unknown in advance, and use it further for characterization of the intermediate layer (in this case, the thickness of the latter does not exceed 600 nm); 2) absence of this narrow peak and availability of a wider B peak is indicative of the fact that the thickness of the intermediate layer exceeds 1000 nm. Then, using the SPR curve one can estimate the thickness d_m and the lower limit of ε_s. In this case, determination of the ε_b value becomes impossible. The absence of peaks in the curve *dR*/*dF* (*F*) shows that the thickness of the intermediate layer lies within the limits 600 < d_m < 1000 nm.

3. Solving the Inverse Task – Representation of the Gradual Intermediate Layer as a Single One with Effective Values of the Thickness and Dielectric Permittivity

In practical applications, one has to solve an inverse problem – to determine a profile of the dielectric permittivity $\varepsilon(x)$ by using the experimental curve $R(F)$. Usually, with this aim in Kretschmann geometry systems they assume availability of one (maximum two) layer between the surface of plasmon-keeping metal and semi-infinite medium (in this case – liquid) and use the fitting procedure for experimental and calculated SPR curves to reach the best coincidence. If one assumes that the intermediate layer between the gold surface and colloidal solution bulk can be described as one layer with effective values of the thickness d and dielectric permittivity ε, it seems reasonable to try to determine d and ε values by using the data of Fig. 3A as the "experimental" ones. This procedure is widely known and multiply described (see, for example [18, 19]). Being based on the Winspall 2.20 program, we realized extraction of d, ε and ε_b by using the SPR curves in Fig. 3A as the experimental ones. The obtained d, ε and ε_b values for q = 0.85 in medium with ε_s = 1.82 are shown in Fig. 4 (curves 1 to 9 on the 2 rows) using a solid line. The initial profile $\varepsilon(x)$ is shown with dashed lines. It is seen that for sufficiently low values of d_m (< 600 nm) the obtained d value is equal approximately to half of d_m, while ε is close to ε_s, exceeding it a little. In the case of thick intermediate layers (d_m > 600 nm), the

obtained d value is significantly lower, and ε possesses some intermediate value between ε_b and ε_s.

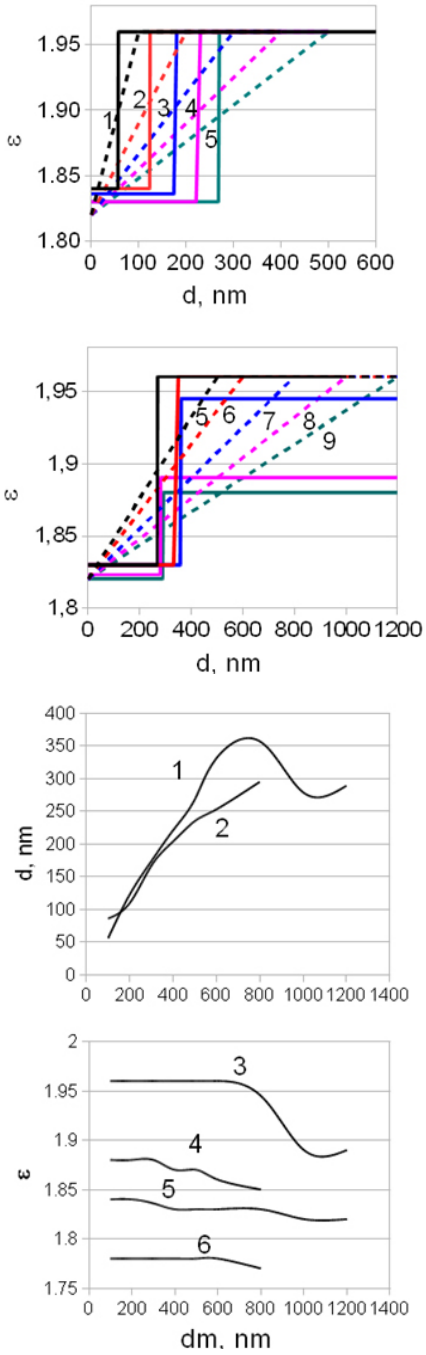

Fig. 4. Top: comparison of the "initial" (dashed lines) and extracted for one layer model (solid lines) for monotonically increased profile ε(x). d_m value is 50, 100, 200, 300, 400, 600, 800, 1000 and 1200 nm for graphs 1...9 accordingly. Bottom: graphs of extracted parameters d (1,2), ε_b (3, 4) ε(5, 6) versus d_m 1, 3, 5 for q= 0.85 (dense suspension); 2, 4, 6 for q= 0.45 (loose suspension).

Our calculations performed for other relations of ε_b and ε_s show the same behavior. In more details, dependences for parameters d, ε, and ε_b on the thickness of intermediate layer d_m are depicted in Fig. 4 (on the bottom) for suspensions of different densities (q = 0.85 and 0.45). Thereof, it follows that d is equal approximately to half of d_m up to 600 nm; after that d slows down and reach the value 300 nm independently of q (curves 1 and 2). The ε value exceeds a little the value ε_s (1.77 or 1.88) practically coinciding with it for d_m > 600 nm. With account of the above features, one can judge the thickness (and dielectric permittivity) of the intermediate layer up to the value 600 nm. It is obvious that, in the case when d_m exceeds 600 nm, the part of the curve within the range of the critical angle (see Figures 3c and 3d) becomes more informative.

4. Experimental

4.1. Equipment and Materials

Measurements of angular dependences for light reflection from the interface suspension/gold film on glass substrate were performed using the SPR spectrometer Plasmon 6 (model 325, ISP NASU, Ukraine) that allows measuring the absolute value of reflectivity as well as absolute value of the angle in Kretschmann configuration. The retro-prism with the base angle 65 degree and glass substrates were made of the glass F-1 with the refraction index 1.61. The wide range of angles for scanning (up to 17 degree in air) allows performing quantitative measurements of a full reflection curve including the TIR and SPR angles for liquids with various refraction indexes – from 1.33 (water) up to 1.41 (haemoglobin).

To measure the SPR effect, glass substrates were covered with a thin gold layer (approximately 50 nm) deposited on the adhesive chromium sub-layer by using thermal evaporation in vacuum. Before investigations, the prepared substrates were kept in dry nitrogen atmosphere. A plastic cell of the volume 30 µl was provided with two plastic pipes of the internal diameter 1 mm that were joined to a digital micro-pump. Preliminary processing the data was realized using the program Plasmon 6 (version 6.7). The operation regime of a "single mode" allows obtaining the full reflection curve for 10 s.

As samples of suspensions, we used heparinized blood taken from a vein of a healthy donor and blood cellular mass after centrifuging. These blood samples were placed into test-tubes containing 0.1 ml of heparin (5000 U/ml, Pharma life, Ukraine) and agitated. To prepare the erythrocyte mass, a part of heparinized blood was centrifuged (10 min, 3000 rev/min). After determination of hematocrit, the top layer of plasma was separated into another test-tube, while the bottom layer of the erythrocyte mass was divided by aliquots of 200 µl that were used for measurements. The samples of suspensions (blood and erythrocyte mass) were kept at the temperature 4 ^{0}C. As a buffer solution, we used the Ringer solution (buffer solution, in what follows). Its composition is as follows: NaCl - 9 g, $NaHCO_3$ - 0.2 g, $CaCl_2$ - 0.2 g, KCl - 0.2 g, glucose -1 g, water - up

to 1 l. Decimolar solution of HCl and distilled water were used to rinse the system and regenerate the operation surface. All the experiments were performed at room temperature.

4.2. Experimental Results

After centrifuging, the whole blood breaks by two ranges: transparent liquid (plasma) is the top one, and dark opaque (erythrocyte mass) is the bottom one. The typical series of the SPR curves obtained for contact of erythrocyte mass with gold for 0…10 min is depicted in Fig. 5a (curves 1 to 6). Immediately after contact, the angle of plasmon resonance is fixed at ~66.8 degree, however, for the first 10 min its position shifts to the left by ~ 0.3 degree and then is stabilized. Near the critical angle (~60.5 degree), one can observe a shoulder typical for the TIR effect, which does not change with time. The curve 7 in Fig. 5a is the SPR curve inherent to transparent liquid (plasma). Here, contrary to the curves 1…6, the F_{min} position is shifted by ~1.5 degree to the left, and the range of the critical angle is shifted down to ~56.1 degree. This curve does not change with time. The curves 8 and 9 are the first derivatives *dR*/*dF* of the curves 1 to 7 near the critical angle. Note that they clearly demonstrate narrow peaks at ~60.4 and ~56.2 degree, respectively. As it was shown earlier, availability of these peaks allows determining the ε_b value in the studied suspension.

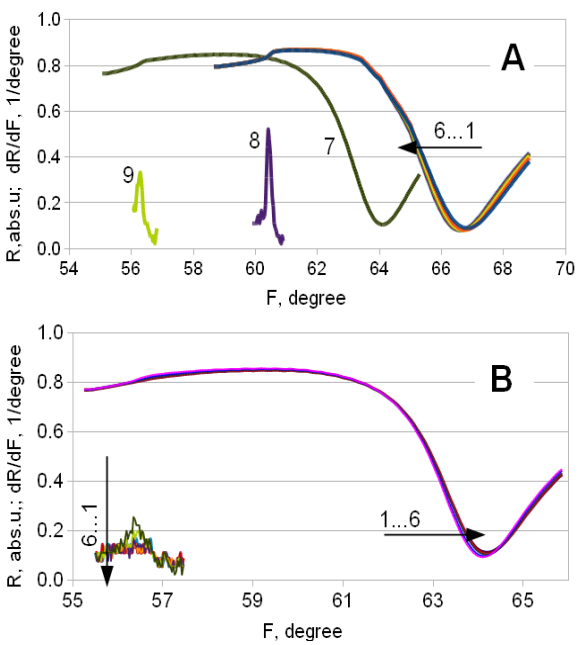

Fig. 5. a) 1-6 repetitive measurements of *R(F)* curves for erythrocyte mass, 7 – *R(F)* curve for plasma. 8, 9 – first derivatives *dR/dF(F)* for erythrocyte mass and plasma accordingly; b) 1 – 6 experimental curves *R(F)* for whole blood (hematocrit ~0,4); bottom left – *dR/dF(F)* for the same specimen (y-scale is three time multiplied).

Depicted in Fig. 5b are the results obtained for the sample of heparinized blood with the hematocrite value 0.4. Contrary to the previous data, the SPR curves for the first 10 min do not diverge. One can see only a small increase in the F_{min} value near 64 degree. As a whole, this curve is close to the curve 7 in Fig. 5a for pure plasma. Near 57 degree, one can see a weak indication of a step and its kinetics as some thickening the line in the plot. (We have marked that changes in the signal value are observed here in the last digit of registering analog-to-digital converter). Shown on the left bottom is derivatives *dR*/*dF* where it is seen that contrary to Fig. 5a the peak is several times wider, and its maximum sharply decreases with time. So, in the first scan, it is approximately equal to 0.07 degree^{-1}, which is practically three-fold higher than the noise level, and already in the fourth scanning (after two minutes) its amplitude drops to the level lower than the noise one. (The scale of these curves is three-fold increased).

4.3. Discussion

Let us analyze the obtained SPR curves from the viewpoint of availability of the intermediate layer.

4.3.1. Dense Suspension (Erythrocyte Mass)

Final results of fitting the parameters *d*, ε and ε_b for the SPR curves corresponding to the contact with dense suspension (Fig. 5a) are summarized in Table 2 (the first six lines). The numbers 1 to 6 correspond to numbers of measuring cycles (they correspond to different times past after sample introduction). The ε value for this layer decreases approximately from 1.87 down to 1.86 in the course of measurements. At the same time, the ε_b value remains practically constant at the level 1.964 ±0.002. This value has been obtained for absolute majority of the samples in the series of 40 investigations. The thickness of an equivalent layer *d* is about 200 nm in the initial moment and decreases down to ~140 nm for 10 min. It should be noted that the main part of this decrease in *d* values takes place in the first minute (cycles 1 and 2). Using the above ε_b value, one can calculate the volume fraction of erythrocytes q_e in erythrocyte mass, if he knows the dielectric permittivities of haemoglobin ε_g and plasma ε_p. The latter can be determined from the experimental data shown in Fig. 5A (curve 9). The angular position of A peak is 56.28±0.01 degree, which corresponds to $\varepsilon_p = 1.793 \pm 0.004$; the ε_g value (see [16]) is 1.979. In this case, the equation (1) leads to q_e values summarized in the last column of Table 2. They lie within the limits 0.9...0.92, which is indicative of rather dense packing the erythrocytes, if taking into account that they possess the shape of oblate torus with the diameter about 8 μm and thickness close to 2 μm [20].

Table 2. Optical parameters d, ε, ε_b recovered from experimental SPR curves by means of fitting with calculated ones.

Cycle number (time)	d, nm	ε	ε_b	q_e
Dense suspension (erythrocyte mass)				
1(0.5 min)	200	1.8725	1.9622	0.9097
2 (1 min)	156	1.8736	1.9656	0.9280
3 (2 min)	144	1.8717	1.9648	0.9237
4 (4 min)	141	1.8701	1.9650	0.9247
5 (6 min)	136	1.8679	1.9645	0.9220
6 (10 min)	132	1.8673	1.9645	0.9220
Loose suspension (whole blood, haematocrit 0.4)				
1A (0,5 min)	1200	1.80	1.88	
2A (1 min)	1100	1.80	1.88	
3A (2 min)	700	1.824	1.88	
4A(4 min)	700	1.8155	1.82	
5A (10 min)	-	-	1.8252	

A simple calculation shows that in assumption when erythrocytes possess the shape of plain cylinder then the factor of filling the space will be $q = \pi/4 = 0.79$ for dense quadratic package, and for the case of hexagonal package $q = 0.9$. The q value found by us exceeds 0.9. Thus, it should be concluded that during centrifuging erythrocytes are deformed under action of hydrostatic pressure and change their round shape to that of polyhedron, which provides a higher level of package than that of plain cylinders. This conclusion has been confirmed by the data [21] where it is shown that after centrifuging erythrocytes are strongly deformed.

Thus, measurements of a SPR curve in a wide range of angles including that of a critical angle allows rather reliable estimation of the dielectric permittivity for a dense suspension of erythrocytes ε_b and then the density of their package q_e. This parameter was not determined earlier and may be important as the erythrocyte package is related with their shape and membrane elasticity, which can carry essential information.

As to the very intermediate layer in the samples of dense package, shown in Fig. 6a is behavior of ε(x) for the first six scans after contact. Solid lines show the results for the model with one effective layer that used instead of plain intermediate layer. Dashed lines show reconstruction of a linear change inherent to ε(x), if using calculations based on Fig. 4.

As it follows from Fig. 6a and Table 2, the effective thickness d of the intermediate layer decreases in the course of interface relaxation from ~200 down to ~140 nm; an especially sharp drop takes place for the first minute. The ε value is decreased, too.

As it was shown in the calculation chapter, in the case of smooth ε growth in the intermediate layer the equivalent thickness of the effective layer d is equal approximately to half of d_m, if the latter does not exceed 600 nm (Fig. 4, on the bottom). In this case, the ε value just on metal surface is close to that of solvent for the case of solid spheres. As the obtained thickness d does not exceed 300 nm, the above rule may be applied to reconstruction of the real dependence ε(x) for the case of dense suspension. The result of this reconstruction is shown in Fig. 6 (on the top) for two situations – at the start of relaxation and at its end (curves 1' and 2', respectively). It is seen that for $x = 0$ the ε value is equal to ~1.87 at the origin and ~1.85 at the end of measurements, which obviously exceeds the ε value for plasma (1.79).

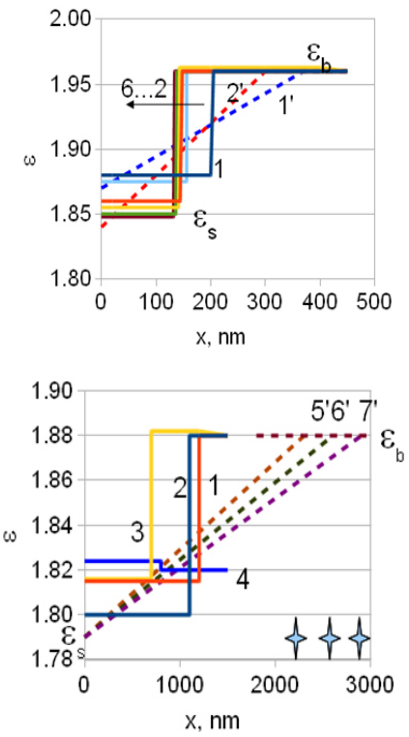

Fig.6. Recovered ε(x) dependencies. A – dense suspension (erythrocyte mass), B- loose suspension (whole blood). Solid lines are obtained for one layer model, dashed lines reflected the reconstruction of linear ε(x) increase based on the result pervious modeling (Fig. 4).

This excess should be related with erythrocyte deformation. As said above, under action of hydrostatic forces in the centrifuge mechanic field the curved surface of a cell converts to polyhedron. It seems natural that plain parts of the cells, which arise under centrifuging, will be first of all turned to the gold surface. As a result, filling the volume in the first layer of this multilayer stack above the surface differs from zero (Fig. 2) and is determined by the total surface of cells being in contact with gold. Using the equation (2), one can find that at the origin of relaxation (profile 1') the area of cell toughing to gold is equal to 0.47 of the total area, while at the end

of the process (profile 2') it is shortened down to 0.35. At the same time, the thickness of the layer d_m decreases from 360 down to 280 nm.

4.3.2. Loose Suspension (whole Blood with the Hematocrit 0.4)

The SPR curves for this case are depicted in Fig. 5B. With regard to the erythrocyte mass, the angle of SPR minimum is shifted to 64 degree inherent to pure plasma, and practically does not change with time. Another feature is the absence of A peak in the dependence *dR*/*dF* near the value 61 degree. Instead of it, there arises a peak near 56.8 degree that can be ascribed to the peak B with account of its width. The absence of A peak in the dependence *dR*/*dF* does not allow determining the value of dielectric permittivity for suspension bulk ε_b. But this value can be calculated using the formula (2) with account of hematocrit. One can obtain $\varepsilon_b = 1.88$, and this value can be used when fitting the experimental and calculated curves. The lines 1, 2 and 3 in Fig. 6B show the results of fitting for the first three scans. If believing to that, then the equivalent thickness of intermediate layer decreases from 1200 down to 700 nm. However, if the ε_b value is not set by calculation, then one can obtain the result shown with the line 4. It means that SPR is not able "to look" further than 600 nm.

Our detailed investigation of the *R*(*F*) near the critical angle allows to shed light on the structure of intermediate layer at the gold surface. Availability of the wide peak in the *dR*/*dF* curve within the range 56.5...56.6 degree enabled us to juxtapose its amplitude with the thickness of intermediate layer d_m that was predicted by calculations performed using Fig. 3d. The result of this juxtaposition is shown in Fig. 6b with four-ray asterisks in positions 5' to 7' where fixed is the thickness of intermediate layer and value of dielectric permittivity directly at the metal surface. If one takes the value $\varepsilon_b = 1.88$, then the profile $\varepsilon(x)$ can be described by the lines 5', 6' and 7', which essentially differs from the result obtained using the SPR curves (plots 1 to 4). In the first moment of blood contact with the gold surface, the d_m value reaches 3 μm and decreases down to 2 μm in the course of relaxation. This process definitely resembles the effect of erythrocyte deposition that is observed in analytical practice in the top part of a capillary. It gives a hope that this process can find the same wide application as the common method for determination of the velocity of erythrocyte concretion, but with the essential difference in time – several minutes instead of hour exposure.

As a conclusive note, we should say that in the case of large (more than several micrometers) colloidal particles, the SPR effect is unable to analyze intermediate layers, and the range of the critical angle becomes predominant. In these conditions, it seems reasonable to reduce the thickness of gold layer with the aim to make the range of critical angle more pronounced. Indeed, from the viewpoint of sensitivity, the optimum gold thickness is 45 to 55 nm, and the reflectivity reaches 80 % within the range of critical angles. Reduction of the gold thickness will allow increasing signals within the TIR range and, at the same time, clearly observing the very SPR effect.

5. Conclusion

Offered in this work is the approach to describe the SPR effect in colloidal systems scattering light. It is based on quantitative calculation of the dielectric permittivity ε both in bulk and near the boundary metal/suspension with account of the Bruggeman theory for effective medium. Introduced is the conception of an intermediate layer with a gradual increase in the ε value from the surface up to the bulk one within the limits of the layer thickness d_m. It has been shown that in the case $d_m < 600$ nm one can quantitatively determine both ε values for suspension bulk and the parameters of the intermediate layer. In the case when $d_m > 1000$ nm, it is possible to estimate the thickness of intermediate layer and the ε value near the surface. To determine the bulk value ε from the SPR curve is impossible in this case. The approach has been illustrated by the results of controlling the dense suspension (weighted erythrocytes) and loose suspension (whole blood). In the former case, we have shown that $d_m < 600$ nm, and it allows determining the bulk ε as well as the degree of filling the suspension bulk with cells. We have made the assumption that the cell shape near the gold surface influences on the contact area with metal, which determines relaxation of intermediate layer parameters. In the latter case, we have been enabled to estimate the thickness of the intermediate layer gold-whole blood. It has been shown that d_m is approximately 2000...3000 nm, and suspension bulk is unavailable to be controlled with SPR. But this control can be possible in the case of lower gold film thicknesses or when it is absent at all when light interference inside a plain ε gradient near the surface of glass substrate becomes a predominant optical effect.

Acknowledgments

This work was supported by scientific projects of NAS of Ukraine "Design and creation of sensor Bioplasm systems for diagnostics, treatment and prevention of cardiovascular, infectious and neurological diseases» and «Analytical devices on the base of Surface Plasmon Resonance for wide application in veterinary, medicine and biological investigation». Authors are much appreciated Dr. Sci. E. Kaganovich and PhD. A. Kudryavtsev for valuable notes to manuscript.

References

[1]. I. Pockrand, Surface plasma oscillations at silver surfaces with thin transparent and absorbing coatings, *Surf. Sci.,* Vol. 32, 1978, pp. 577–580.

[2]. H. Raether, Surface plasmons on smooth and rough surfaces and on gratings, in Tracts in Modern Physics. *Springer Verlag*, Berlin, Germany, 1986, Vol. 111.

[3]. H. E. de Bruijin, B. S. F. Altenburg, R. P. H. Kooyman, and J. Greve, Determination of film thickness and dielectric constant of thin transparent dielectric layers using surface plasmon resonance, *Opt. Commun.,* Vol. 82, 1991, pp. 425–430.

[4]. K. Matsubara, S. Kawata, and S. Minami, Optical chemical sensor based on surface plasmon measurement, *Appl. Opt.,* Vol. 27, 1988, pp. 1160–1163.

[5]. B. Liedberg, C. Nylander, and I. Lundström, Surface plasmon resonance for gas detection and biosensing, *Sens. Actuators B*, Vol. 4, 1991, pp. 299–304.

[6]. A. Schilling, O. Yavas¸, J. Bischof, J. Boneborg, and P. Leiderer, Absolute pressure measurement on nanosecond scale using surface plasmons, *Appl. Phys. Lett.,* Vol. 69, 1996, pp. 4159–4161.

[7]. P. Pfeifer, U. Aldinger, G. Schwotzer, S. Diekman, and P. Steinrücke, Real time sensing of specific molecular binding using surface plasmon resonance spectroscopy, *Sens. Actuators B*, Vol. 54, 1999, pp. 166–175.

[8]. S. Herminghaus and P. Leiderer, Nanosecond time resolved study of pulsed laser ablation in the monolayer regime, *Appl. Phys. Lett.,* Vol. 58, 1991, pp. 352–354.

[9]. J. Homola, S. S. Yee, and G. Gauglitz, Surface plasmon resonance sensors: Review, *Sens. Actuators B*, Vol. 54, 1999, pp. 3–15.

[10]. A. Otto, Excitation of nonradiative surface plasma waves in silver by the method of frustrated total reflection, *Z. Phys.,* Vol. 216, 1968, p. 398.

[11]. E. Kretschmann and H. Raether, Radiative decay of nonradiative surface plasmons excited by light, *Z. Phys.,* Vol. 239, 1968, p. 2135.

[12]. John G. Quinn, S. O'Neill, A. Doyle, C. McAtamney, D. Diamond, B. D. MacCraith and R. O'Kennedy Development and Application of Surface Plasmon Resonance-Based Biosensors for the Detection of Cell-Ligand Interactions, *Analytical Biochemistry,* 281, 2000, pp. 135–143.

[13]. D. E. Aspnes, Optical properties of thin films, *Thin Solid Films,* 89, 1982, pp. 249-255.

[14]. A. V. Goncharenko, Generalizations of the Bruggeman equation and a concept of shape-distributed particle composites, *Physical Review E*, 68, 2003, 041108.

[15]. N. L. Dmitruk, A. V. Goncharenko, E. F. Venger, Optics of small particles and composite media, *Naukova Dumka,* Kyiv, 2009, 386 p.

[16]. M. Meinke, G. Müller, J. Helfmann, M. Friebel Optical properties of platelets and blood plasma and their influence on the optical behavior of whole blood in the visible to near infrared wavelength range, *Journal of Biomedical Optics,* 12, 1, 2007, 014024.

[17]. M. Friebel and M. Meinke, Determination of complex refractive index of highly concentrated haemoglobin solutions using transmittance and reflectance measurements, *Journ. Biomed. Opt.,* 10, 6, Nov/Dec 2005, 064019.

[18]. S. Ekgasit, A. Tangcharoenbumrungsuka, F. Yu., A. Baba, W. Knoll Resonance shifts in SPR curves of non-absorbing, weakly absorbing, and strongly absorbing dielectrics, *Sensors and Actuators B: Chem.,* 105, 2005, pp. 532–541.

[19]. G. V. Beketov, Yu. M. Shirshov, O. V. Shynkarenko, V. I. Chegel, Surface plasmon resonance spectroscopy: prospects of superstrate refractive index variation for separate extraction of molecular layer parameters, *Sensors and Actuators B: Chem.,* 48, 1998, pp. 432-438.

[20]. Anthea M., Hopkins J., McLaughlin C. W., Johnson S., Warner M. Q., LaHart D., Wright J. D., Human Biology and Health, *Prentice Hall,* Englewood Cliffs, New Jersey, USA, 1993.

[21]. W. V. Miller, M. J. Wilson Effects of Centrifugation on Erythrocytes, *Transfusion,* Vol. 14, No. 3, 1974, pp. 278–282.

The Fourth International Conference on Sensor Device Technologies and Applications

SENSORDEVICES 2013

25 - 31 August 2013 - Barcelona, Spain

Tracks: Sensor devices - Ultrasonic and Piezosensors - Photonics - Infrared - Gas Sensors - Geosensors - Sensor device technologies - Sensors signal conditioning and interfacing circuits - Medical devices and sensors applications - Sensors domain-oriented devices, technologies, and applications - Sensor-based localization and tracking technologies - Sensors and Transducers for Non-Destructive Testing

Deadline for papers: 30 March 2013

http://www.iaria.org/conferences2013/SENSORDEVICES13.html

The Seventh International Conference on Sensor Technologies and Applications

Deadline for papers: 30 March 2013

SENSORCOMM 2013

25 - 31 August 2013 - Barcelona, Spain

Tracks: Architectures, protocols and algorithms of sensor networks - Energy, management and control of sensor networks - Resource allocation, services, QoS and fault tolerance in sensor networks - Performance, simulation and modelling of sensor networks - Security and monitoring of sensor networks - Sensor circuits and sensor devices - Radio issues in wireless sensor networks - Software, applications and programming of sensor networks - Data allocation and information in sensor networks - Deployments and implementations of sensor networks - Under water sensors and systems - Energy optimization in wireless sensor networks

http://www.iaria.org/conferences2013/SENSORCOMM13.html

The Sixth International Conference on Advances in Circuits, Electronics and Micro-electronics

CENICS 2013

25 - 31 August 2013 - Barcelona, Spain

Deadline for papers: 30 March 2013

Tracks: Semiconductors and applications - Design, models and languages - Signal processing circuits - Arithmetic computational circuits - Microelectronics - Electronics technologies - Special circuits - Consumer electronics - Application-oriented electronics

http://www.iaria.org/conferences2013/CENICS13.html

Aims and Scope

Sensors & Transducers is a peer reviewed international, interdisciplinary journal that provides an advanced forum for the science and technology of physical, chemical sensors and biosensors. It publishes original research articles, timely state-of-the-art reviews and application specific articles with the following devices areas:

- Physical, chemical and biosensors;
- Digital, frequency, period, duty-cycle, time interval, PWM, pulse number output sensors and transducers;
- Theory, principles, effects, design, standardization and modeling;
- Smart sensors and systems;
- Sensor instrumentation;
- Virtual instruments;
- Sensors interfaces, buses and networks;
- Signal processing and interfacing;
- Frequency (period, duty-cycle)-to-code converters, ADC;
- Technologies and materials;
- Nanosensors;
- Microsystems;
- Applications.

Further information on this journal is available from the Publisher's web site:
http://www.sensorsportal.com/HTML/DIGEST/Submission.htm

Subscriptions

An annual subscription includes 12 regular issues and some special issues. Annual subscription rates for 2013 are the following:

Electronic version (in printable pdf format): 400.00 EUR
Printed with b/w illustrations: 640.00 EUR
Printed full color version: 760.00 EUR

40 % discount is available for IFSA Members.

Prices include shipping costs by mail. Further information about subscription is available through IFSA Publishing's web site: http://www.sensorsportal.com/HTML/DIGEST/Journal_Subscription.htm

Advertising Information

If you are interested in advertising or other commercial opportunities please e-mail sales@sensorsportal.com and your enquiry will be passed to the correct person who will respond to you within 24 hours. Please download also our Media Planner 2013: http://www.sensorsportal.com/DOWNLOADS/Media_Planner_2013.pdf

Books for Review

Publications should be sent to the IFSA Publishing Office: Ronda de Ramon Otero Pedrayo, 42C, 1-5, 08860, Castelldefels, Barcelona, Spain.

Abstracting Services

This journal is cited, indexed and abstracted by Chemical Abstracts, EBSCO Publishing, IndexCopernicus Journals Master List, ProQuest Science Journals, CAS Source Index (CASSI), Ulrich's Periodicals Directory, Scirus, Google Scholar, etc. Since 2011 *Sensors & Transducers* journal is covered and indexed by EI Compendex index (including a Scopus, Embase, Engineering Village and Reaxys) in *Elsevier* products.

Instructions for Authors

Please visit the journal web page http://www.sensorsportal.com/HTML/DIGEST/Submission.htm Authors must follow the instructions very carefully when submitting their manuscripts. Manuscript must be send electronically in both: MS Word 2003 for Windows (doc) and Acrobat (pdf) formats by e-mail: editor@sensorsportal.com